Journal of Molecular Liquids 437 (2025) 128596

Contents lists available at ScienceDirect

Journal of Molecular Liquids

journal homepage: www.elsevier.com/locate/molliq

Impact of amylenes in dipeptide-mediated phospholipid vesicle integrity and aggregation

Martín Eduardo Villanueva [a], Jacobo Troncoso [b], Patricia Losada-Pérez [a,*], Aida Jover [c,*]

[a] Experimental Soft Matter and Thermal Physics (EST) Group, Department of Physics, Université libre de Bruxelles, Boulevard du Triomphe CP223, 1050 Brussels, Belgium
[b] Instituto de Física e Ciencias Aeroespaciais, Departamento de Física Aplicada, Universidade de Vigo, Campus As Lagoas, 32004 Ourense, Spain
[c] Departamento de Química Física, Universidade de Santiago de Compostela, Facultade de Ciencias, Alfonso X o Sabio s/n, 27002 Lugo, Spain

ARTICLE INFO

Keywords:
Lipid vesicles
Diphenylalanine
Amylene
Vesicle aggregation
Model membrane organization

ABSTRACT

Interactions between lipid membranes are central to biological, biochemical, and biophysical processes. While adhesion between intact vesicles typically requires complex molecular linkers to overcome electrostatic and hydration repulsions, aggregation involves bilayer disruption and loss of vesicle integrity, a phenomenon more often associated with pathology. Here we report a minimal and straightforward route to induce aggregation of zwitterionic vesicles through the combined action of diphenylalanine (Phe-Phe), a dipeptide motif of the Alzheimer's β-amyloid peptide, and amylene, a small apolar alkene used as a chloroform stabilizer. Using NMR spectroscopy, microscopy, and thermodynamic and nanomechanical characterization, we demonstrate that Phe-Phe alone perturbs bilayer organization only mildly, but in the presence of amylene it synergistically drives membrane disruption and vesicle aggregation. These results highlight how the interplay of small molecules can reorganize zwitterionic membranes and eventually induce spontaneous aggregation.

1. Introduction

Phospholipid vesicles are widely used as surrogates for cell membranes in biophysical studies and as platforms for drug delivery and microreactors [1–3]. Their interactions can lead to several distinct outcomes, including fusion, which underlies processes such as neurotransmitter release and viral entry [4,5], and aggregation, which is often associated with pathological lipid–protein assemblies in atherosclerosis and Alzheimer's disease [6,7]. Understanding these processes is therefore essential both for elucidating disease mechanisms and for designing functional soft materials such as tissue mimics.

The physical basis of vesicle–vesicle interactions is commonly described by DLVO theory (Derjaguin–Landau–Verwey–Overbeek) and its modifications, which balance attractive van der Waals forces against electrostatic and hydration repulsions [8–10]. For charged vesicles, aggregation can be induced by charge neutralization through the addition of salts, pH adjustment, or multivalent cations [10–13]. Once the repulsive barrier is reduced, the residual van der Waals attraction drives clustering, although such aggregation often remains dynamic and reversible due to lipid rearrangements and charge redistribution [11].

In contrast, zwitterionic vesicles are stabilized mainly by short-range hydration forces between lipid headgroups, which impose a strong repulsion at nanometer-scale separations. Because van der Waals attraction alone is insufficient to overcome this barrier, spontaneous aggregation of zwitterionic vesicles is highly unfavorable. Classical strategies to bring such vesicles into contact rely instead on external linkers that promote adhesion while preserving vesicle integrity. Examples include complementary DNA strands grafted to lipid headgroups [14] and biotin–avidin cross-bridges [15]. Adhesion of intact vesicles is biologically relevant but requires delicate molecular control.

By contrast, aggregation involves the disruption of vesicle morphology, sometimes leading to collapse, fragmentation, or the formation of irregular aggregates rather than stable contacts between intact vesicles. This type of membrane-disruptive aggregation has been mainly observed with antimicrobial peptides and amyloid fibrils [16–18]. Small amphiphilic molecules can also induce vesicle aggregation at sufficiently high concentrations: ethanol promotes aggregation and fusion of phosphatidylcholine vesicles through bilayer interdigitation [19], while DMSO collapses zwitterionic vesicles into multilamellar or non-spherical structures [20]. These examples illustrate that, although possible, aggregation of zwitterionic vesicles generally requires either high concentrations of small molecules or the action of large peptides

* Corresponding authors.
E-mail addresses: patricia.maria.losada.perez@ulb.be (P. Losada-Pérez), aida.jover@usc.es (A. Jover).

https://doi.org/10.1016/j.molliq.2025.128596
Received 22 February 2025; Received in revised form 7 September 2025; Accepted 22 September 2025
Available online 23 September 2025

and proteins.

In this work, we focus on the interplay between a short alkene and a minimal peptide motif in driving the organization and eventual aggregation of model 1,2-dimyristoyl-sn-glycero-3-phosphocholine (DMPC) vesicles. As small molecule we chose amylene, a completely apolar chloroform stabilizer used to prevent degradation and the formation of phosgene, a highly toxic compound [21]. As peptide we used diphenylalanine (Phe-Phe), a dipeptide well known for forming hollow tubular assemblies and for being the core motif of the Alzheimer's β-amyloid peptide [22]. In previous work we showed that Phe-Phe interacts with DMPC bilayers in a concentration-dependent manner: at low concentrations it has little effect, whereas at higher concentrations it promotes mild weakening of bilayer organization and stability, likely by locating at the headgroup–water interface and occasionally inserting into the hydrophobic core [23,24]. Here we use a combination of thermodynamic, nanomechanical, microscopy, and spectroscopic approaches to show that in the presence of amylene, Phe-Phe induces clear membrane disruption and a strong tendency towards vesicle aggregation, consistent with the formation of intermembrane amylene-Phe-Phe complexes.

2. Materials and methods

2.1. Sample preparation

DMPC lipid in powder form was purchased from Avanti Polar Lipids (Alabaster, AL) and di-*L*-phenylalanine from Sigma-Aldrich. Two chloroform types were used, one stabilized with 100–200 ppm of amylenes, with purity better than 0.995 in mass fraction, and the other one stabilized with 0.4–0.6 % of ethanol, with purity greater than 0.999 in mass fraction. The samples at the different peptide-lipid ratios (P/L) were prepared both in ethanol and in amylene-stabilized chloroform as dispersant solvent for comparison. We found that the volume of ethanol-stabilized chloroform used for dissolving the powders is irrelevant, yet this was not the case for the amylenes-stabilized one. Therefore, aliquots of a diphenylalanine chloroform solution at 0.13 mg/ml were added to the required volumes of DMPC chloroform solutions at 10 mg/ml in order to reach the P/L weight ratios to be studied. The amount of amylene goes up to 0.35 mg per DMPC mg for the most concentrated diphenylalanine solutions. For the sake of comparison, some samples were prepared using a smaller chloroform volume (see sections 3.3–3.5). Multilamellar vesicles were subsequently prepared following previously reported standard procedures [24]. P/L mixed films were formed by drying the mixed components in the organic solvent with a gentle N_2 stream and 48 h vacuum. Then, the films were hydrated in Milli-Q water to form stock solutions at 2 mg/ml (QCM-D and AFM) and 10 mg/ml (density, heat capacity, microscopy and NMR experiments) under continuous stirring for 45 min, in a temperature-controlled water bath at 40 °C. When needed, dilutions of the above-mentioned stock solutions were properly carried out to reach the final working concentrations.

2.2. Langmuir isotherms

Langmuir films of DMPC and Phe-Phe/DMPC mixtures were obtained by spreading an aliquot of each sample at the air-water interface of a Langmuir trough using a Hamilton microsyringe (precise to ±0.25 μl). Solutions were prepared using either ethanol- or amylene-stabilized chloroform. Phe-Phe/DMPC mixtures at 0.05, 0.1, and 0.2 P/L ratios were obtained by mixing proper volumes of the respective stock solutions. The total number of molecules in the mixed monolayers (5×10^{16}) was kept constant in all the experiments. The surface pressure-area (π–A) isotherms were obtained in Milli-Q water on a KSV 2000 L balance (KSV, Helsinki, Finland) equipped with a Wilhelmy-type pressure measuring system. The film compression (using a barrier speed of 10 mm/min) was initiated 5 min after the spreading step in order to ensure total evaporation of the solvent. The temperature of the aqueous subphase was held constant at 25 ± 1 °C with a Lauda E200 circulating water bath (Lauda Königshofen, Germany). The absence of surface-active impurities in the spreading solvent and aqueous subphase was routinely checked before each run, as reported elsewhere. [25] At least three π vs A isotherms were measured, and reproducibility was within a maximum standard error of the mean of 1 mN/m for the surface pressure and under 1 % of the mean area.

2.3. Vibrating tube densitometry

The density of multilamellar vesicles was measured using a high precision DMA5000 densimeter (Anton Paar, Austria). Temperature ramps were carried out upon heating with a step of 0.1 °C. From raw density data, three relevant quantities can be calculated, namely the bulk transition temperature T_m, the width of the transition W_d, and the volume change during the transition between gel and fluid phases. T_m can be determined by identifying the peak in the derivative of the density versus temperature curves. From this curve, the width of the transition peak W_d, a quantity representative of the degree of the cooperativity in the phase change, can be also obtained. The change in volume upon the transition, Δv_m is obtained through the calculation of the specific volume, v_s, using the formula:

$$v_s = \frac{1}{c}\left(\frac{1}{\rho_d} - \frac{1-c}{\rho_s}\right) \quad (1)$$

where ρ_d and ρ_s are the density of the solution and solvent, respectively, and c is the concentration of the lipid in weight fraction. v_s was fitted against temperature to a straight line well above and below the phase transition, and the transition volume was calculated as the height between the two lines at the transition temperature. Uncertainties in T_m, W_d, and Δv_m, were estimated in 0.3 °C, 0.4 °C, and 0.004 $cm^3 \cdot g^{-1}$, respectively. Details about the calculation procedure and experimental methodology are given elsewhere in refs. [24,26].

2.4. Differential scanning calorimetry

Calvet differential scanning calorimetry was used to determine T_m and enthalpy Δh_m of the gel-fluid phase transition. Temperature ramps of 0.25 °C·min^{-1} were used in all the experiments. Calibration was carried out using dry air and water, their heat capacity values being obtained from [27]. The reference cell was filled with water in all experiments. T_m was obtained from the maximum of the peak of the heat capacity versus temperature curves, whereas the transition heat was determined by integrating the heat capacity peak after subtracting the baseline. Uncertainties in T_m, and Δh_m, were estimated in 0.3 °C and 3 kJ·mol^{-1}, respectively. The reported bulk T_m value was estimated to be the mean value of those obtained from calorimetry and densitometry. A more detailed explanation of this methodology is given in [24].

2.5. Quartz crystal microbalance with dissipation monitoring (QCM-D)

A Qsense E4 instrument (Biolin Scientific, Sweden) measuring frequency and dissipation changes for different odd overtones, Δf/n and ΔD (with n, the overtone number) has been used. AT-cut quartz crystals with Au coating (diameter 14 mm, thickness 0.3 mm, quoted surface roughness <2 nm, and resonant frequency 4.95 MHz) were employed. The Au-coated quartz sensors were cleaned for 5 min with a 5:1:1 mixture of Milli-Q water, ammonia and hydrogen peroxide heated at 70 °C, UV-ozone treated with a UV-ozone cleaner (Bioforce Nanosciences, Germany) for 15 min, rinsed in Milli-Q water and dried with N_2. The changes in Δf/n and ΔD were monitored at five different overtones (from 3rd to 11th). The lipid vesicles were injected into the QCM-D cells with a flow rate of 50 μl/min. Vesicle adsorption onto the Au-coated sensors was carried out at 16 °C, the temperature stability at constant temperature being in the order of ±0.02 °C. A baseline with Milli-Q water was first established and lipid vesicles were injected afterwards

over the Au-coated sensor chips. After reaching a stable supported vesicle layer the pump was switched off and the ensemble was left to stabilize for 30 min. Heating scans from 16 to 35 °C were then performed at a rate of 0.4 °C/min. Usually, phase transitions are characterized by a finite jump in both frequency and dissipation temperature dependent signals. [28,29] Their temperature derivative thus yields extrema, providing a straightforward way for determining the onset and completion temperatures of the transition.

2.6. Contact angle measurements

Contact angle (CA) measurements were carried out using an Attension ThetaLite from Biolin Scientific (Sweden) based on the sessile drop method in order to determine the wettability of Au-coated surfaces used during QCM-D experiments. A 3 μL drop of Milli-Q water was dispensed onto clean, UV-ozone treated Au-coated sensor, and the shape of the drop formed on the surface was analysed. The average of all contact angles measured for each Au-coated surfaces was estimated to be 28 ± 5°.

2.7. Atomic force microscopy with force spectroscopy

Supported lipid bilayers (SLBs) were formed by incubating for 15 min DMPC or Phe-Phe/DMPC vesicle suspensions onto very flat SiO_2 at 45 °C inside an INCU-Line® 68R incubator (VWR chemicals, Leuven Belgium). Prior to the AFM measurements, the SiO_2 surfaces were rinsed with MilliQ water avoiding SLB dewetting. AFM imaging and nanomechanical measurements were performed using a JPK Nanowizard 4 BIO-AFM from Bruker (Nano GmbH, Berlin, Germany). All the measurements were performed in milli-Q water at room temperature in an AFM fluid cell. Triangular silicon nitride MLCT-E cantilevers (Bruker, Nano GmbH, Berlin, Germany) with quoted cantilever length of L ~ 140 μm, resonance frequency f ~ 38 kHz, nominal spring constant k ~ 0.1 N/m and nominal tip radius of 20 nm were used. The AFM cantilever was calibrated in Milli-Q water against a clean glass slide according to the thermal noise method. [30] QI images (using quantitative imaging mode) were recorded at different scan sizes using a pixel sampling of 256 × 256, cantilever speed of 45 μm/s, and setpoint force of 300 pN. In order to evaluate and compare the nanomechanical properties of Phe-Phe/DMPC SLBs prepared from lipid films with and without amylenes, force maps over square grids with 16 × 16 points were determined, with a force curve recorded per point. For each sample, several square grids were performed in different regions of the surface to check the homogeneity of the results. A force setpoint of 10 nN and approach speed of 1 μm/s were used. The AFM images were analysed using the JPK Data Processing software®, where the micrographs were flattened using the appropriate lowest order of levelling for each image.

Force spectroscopy measurements were carried out at the same temperature as AFM imaging ($T = 25$ °C) at different tip approach velocities and, as it is shown in the results section, with setpoint forces between 10 and 20 nN. [30] The penetration of the AFM tip through a SLB can be modelled as a two-state process: the tip on top of the bilayer and the tip in contact with the underlying solid surface. These states are separated by an energy barrier that is reduced by the application of an external force and that can be linked to the resistance to rupture of the SLB and thus to the strength of lateral interactions between their constituent molecules. [31] By varying the tip-sample approach speed v and calculating the corresponding average breakthrough force F_b at each speed, it is possible to determine the probability of bilayer rupture that is directly related to the aforementioned energy barrier involved in this process. The model that predicts the logarithmic dependence of F_b with the approach speed can be then fitted according to Eq. 2 as:

$$F_b = a + b\log\frac{v}{v_0} \tag{2}$$

where F_b, a and b are in nN and $v_0 = 1$ μm/s. The fitting parameters a and b can then be inserted in the next equation:

$$k_0 = 1.596\frac{Kv_0}{b}10^{-\frac{a}{b}}, \tag{3}$$

which evaluates the frequency k_0 at which a hole is spontaneously formed in the SLB.

2.8. Bright-field optical microscopy (BFOM)

The multilamellar vesicle dispersions used during bright field optical microscopy were maintained below 15 °C and resuspended with a Pasteur pipette. A drop was deposited on a slide together with a coverslip. The samples were imaged using a Nikon E800 optical microscope at different magnifications depending on the size of the vesicles, employing dry objective lenses of 10× and 20× for the larger sizes and immersion objective lenses of 40×, 60× and 100× for the smaller vesicles. A Nikon DS-U2 digital camera assisted by the NIS-Elements D 2.30 SP1 software was used to acquire the images.

2.9. Confocal laser scanning microscopy (CLSM)

Fluorescent dyes Fast Green FCF (ThermoFisher >95.0 %, $\lambda_{excitation}$ = 635 nm and $\lambda_{emission}$ = 650–710 nm) and Rhodamine B (Sigma-Aldrich ≥95 %, $\lambda_{excitation}$ = 532 nm and $\lambda_{emission}$ = 600–700 nm) were used, since they bound to diphenyalanine and DMPC, respectively. Samples were mixed with both fluorescent dyes a few minutes before the measurement in a final concentration of 5 μg/ml Fast Green FCF and 2.5 μg/ml Rhodamine B. A Leica TCS SPE confocal microscope (Leica Microsystems GmbH, 35578 Wetzlar Germany), equipped with three solid-state lasers with wavelengths 488 nm, 532 nm and 635 nm was used to obtain digital images with 1024 × 1024 pixels resolution.

2.10. Transmission electronic microscopy (TEM)

A 2.5 μL droplet of multilamellar vesicle dispersion was deposited on Formvar/Carbon supported copper grids with 400 mesh size. Uranyl acetate, widely used in TEM to image phospholipid membranes, was added to the solution. [32] Specifically, a drop of 2 % aqueous uranyl acetate was deposited on top of the sample for 30 s, the excess removed with a Whatman filter. The dried samples were examined using a JEOL JEM-1400 Flash (80 kV) (JEOL, Japan) equipped with a JEOL EM-14661 FLASH camera assisted by the TEM Center Ver.1.7.20 software.

2.11. Nuclear magnetic resonance (NMR)

^{1}H NMR spectra were recorded using two Bruker spectrometers, a Bruker AVANCE DPX600 (600 MHz) and on a Bruker AVANCE DPX400 (400 MHz), at 15 °C and 30 °C. At these two temperatures, DMPC is in the gel and fluid phase, respectively. Chemical shifts are reported in ppm from tetramethylsilane (TMS) with the solvent resonance as the internal standard (water 95 % D_2O 5 %, 4.79 ppm). Bidimensional COSY and ROESY experiments were used for the signal assignment.

3. Results and discussion

3.1. Monolayers at the air-water interface

The molecular organization of pure DMPC and Phe-Phe/DMPC mixtures (containing either ethanol or amylenes as chloroform stabilizer) was studied using Langmuir monolayer films. Surface pressure π vs area isotherms are depicted in **Fig. 1a**. As shown by the black solid and dashed lines, DMPC displays its typical liquid-expanded (LE) phase over the entire compression isotherm, both for the amylenes and the ethanol-containing chloroform solutions. This indicates that the interfacial

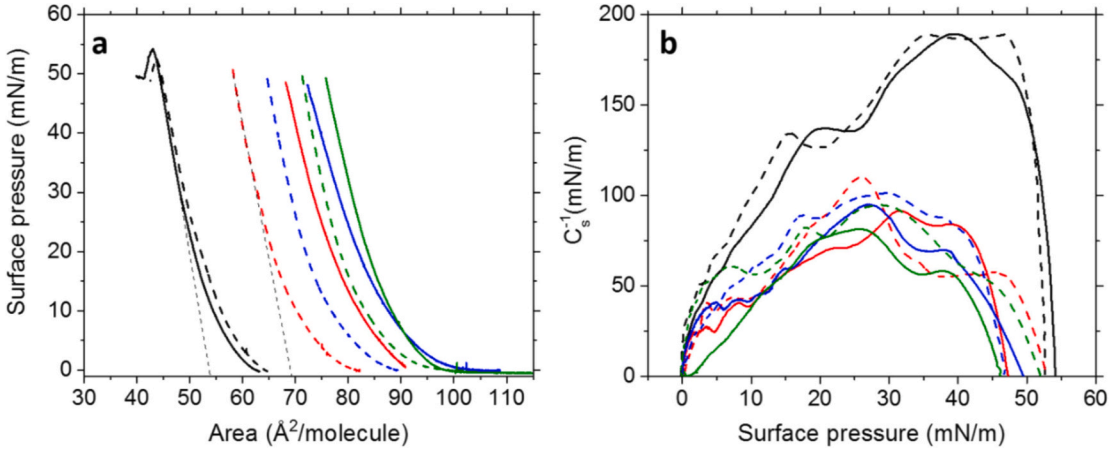

Fig. 1. π-A isotherms (**a**) and variations in the surface compressional modulus (C_s^{-1}) with the surface pressure (**b**), for DMPC and Phe-Phe/DMPC in ethanol- (dashed lines) and amylenes- (solid lines) containing chloroform solutions. The colour code of the lines denoting the different P/L ratios is read as follows: pure lipid (P/L ratio = 0, black), 0.05 (red), 0.1 (blue), and 0.2 (green). Exemplary extrapolating lines to π = 0 are drawn for the pure DMPC and P/L = 0.05 (amylenes containing) isotherms to show the estimated molecular limiting areas (A_{lim}). Experiments were carried out at T = 25 °C.

organization of the pure DMPC monolayer is not sensitive to the preparation method (using ethanol-stabilized or amylene-stabilized chloroform). Subsequently, two sets of samples composed of Phe-Phe/DMPC mixtures prepared using ethanol or amylenes stabilizers were studied. Significant changes on the molecular areas can be observed between the isotherms of Phe-Phe/DMPC mixtures monolayers formed using ethanol-stabilized (dashed lines) and amylene-stabilized (solid lines) chloroform. Several repetitions of the samples at the different P/L ratios allowed us to confirm that peptide/lipid mixtures in the presence of amylenes do experience a greater shift towards higher molecular areas than in the absence of this stabilizer. Thus, while the peptide is able to interact with DMPC membranes causing their expansion in both solvents, this effect is enhanced when amylene-stabilized chloroform was used. To better rationalize this trend, the limiting areas (A_{lim} *i.e.,* the mean molecular area that would be covered by each lipid molecule at zero pressure) were extracted and included in Table 1 for each of the tested samples. Thus, taking the difference between the area shifts for ethanol-stabilized and amylenes-stabilized samples (ΔA_{lim}) an average shift in molecular areas of about ~10 Å^2/molecule was systematically observed in all the cases.

The surface compressional modulus, a quantity that reflects variations of the monolayer's in–plane elasticity, was calculated according to:

$$C_s^{-1} = -A\left(\frac{\partial \pi}{\partial A}\right)_T, \quad (4)$$

where C_s^{-1} is the reciprocal of the compressibility and π is the surface pressure measured at each area point of the isotherm. [33] Variations in the compressional moduli vs π profiles can be directly linked to changes in the elastic properties of films. As shown in **Fig. 1b**, DMPC lipid films experience a significant decrease in the C_s^{-1} at all the surface pressures after the peptide incorporation. Extraction of the maximum compressibility modulus ($C_{s\,max}^{-1}$) from each of the obtained C_s^{-1} vs π profiles enables a better comparison of the results (see Table 1). Similarly to what was observed from the area shifts, the incorporation of a small amount of the peptide (P/L ratio = 0.05) is enough to produce an important decrease in the $C_{s\,max}^{-1}$ (between 70 and 98 mN/m over the value of the pure DMPC). A further decrease in the $C_{s\,max}^{-1}$ values was obtained for all the samples containing amylenes. These differences become clearer when calculating $\Delta C_{s\,max}^{-1} = C_{s\,max}^{EtOH} - C_{s\,max}^{Amylene}$, which ranged from ~7 to 18 mN/m. This implies that amylenes would be able to associate and stabilize along the lipid-peptide joint at the air/water interface. The presence of amylenes thus enhances the expansion effect of the peptide and further increases the fluidity of the lipid membrane, resulting in a more compressible monolayer. It is worth noting that, due to the amphiphilic nature of Phe-Phe, the interactions at the air/water interface are highly dynamic. Therefore, the observed fluctuations on the area and compressibility values at increasing P/L ratios could be caused by partial desorption of molecules towards the interface, depending on the equilibrium between the species.

Control experiments on pure Phe-Phe led to no interfacial activity given the poor adsorption of Phe-Phe in all the solvents. Therefore, only the mixtures with the DMPC lipid were assayed to ensure repeatability (see **Fig. S1**). Considering that the rest of the variables that could potentially play a role on the interfacial behavior (*i.e.*, concentration, temperature, subphase, spread volumes, etc.), were kept constant, this suggests that amylenes somehow help modulating the interaction between the peptide and the lipid.

Table 1
Estimated limiting molecular areas (A_{lim}) and maximum compressibility modulus ($C_{s\,max}^{-1}$) for Phe-Phe/DMPC samples at the assayed P/L ratios.

P/L Ratio	A_{lim} (Å^2/molecule)			$C_{s\,max}^{-1}$ (mN/m)		
	EtOH	Amylene	ΔA_{lim}	EtOH	Amylene	$\Delta C_{s\,max}^{-1}$
0	55.3 ± 0.4	54.8 ± 0.2	–	189.3	189.2	–
0.05	69.1 ± 0.1	82.0 ± 0.5	12.9 ± 0.6	110.3	91.6	18.7
0.10	76.2 ± 0.4	88.1 ± 0.2	11.9 ± 0.6	101.5	95.0	6.5
0.20	81.7 ± 0.3	88.8 ± 0.4	7.1 ± 0.8	94.8	81.5	13.3

3.2. Phase behavior of multilamellar vesicles in bulk

Bulk phase behavior of multilamellar vesicles containing either DMPC or DMPC with Phe-Phe was assessed using calorimetry and densitometry. Fig. 2 highlights the differences obtained in melting temperatures (ΔT_m), enthalpy and volume jumps at the transition (Δh_m and Δv_m), and width of the phase transition (W_d) using both techniques. DMPC and Phe-Phe mixtures prepared using amylene-stabilized chloroform show a much stronger decrease in ΔT_m, Δh_m, and Δv_m and increase in W_d with increasing P/L ratio than their analogues prepared using ethanol-stabilized chloform. This difference is especially significant for the transition enthalpy. These results suggest that the addition of Phe-Phe disrupts the lipid membrane structure, an effect that is significantly amplified by the presence of amylene as stabilizer. Thus, the decrease in T_m with increasing P/L ratio is more pronounced, and the

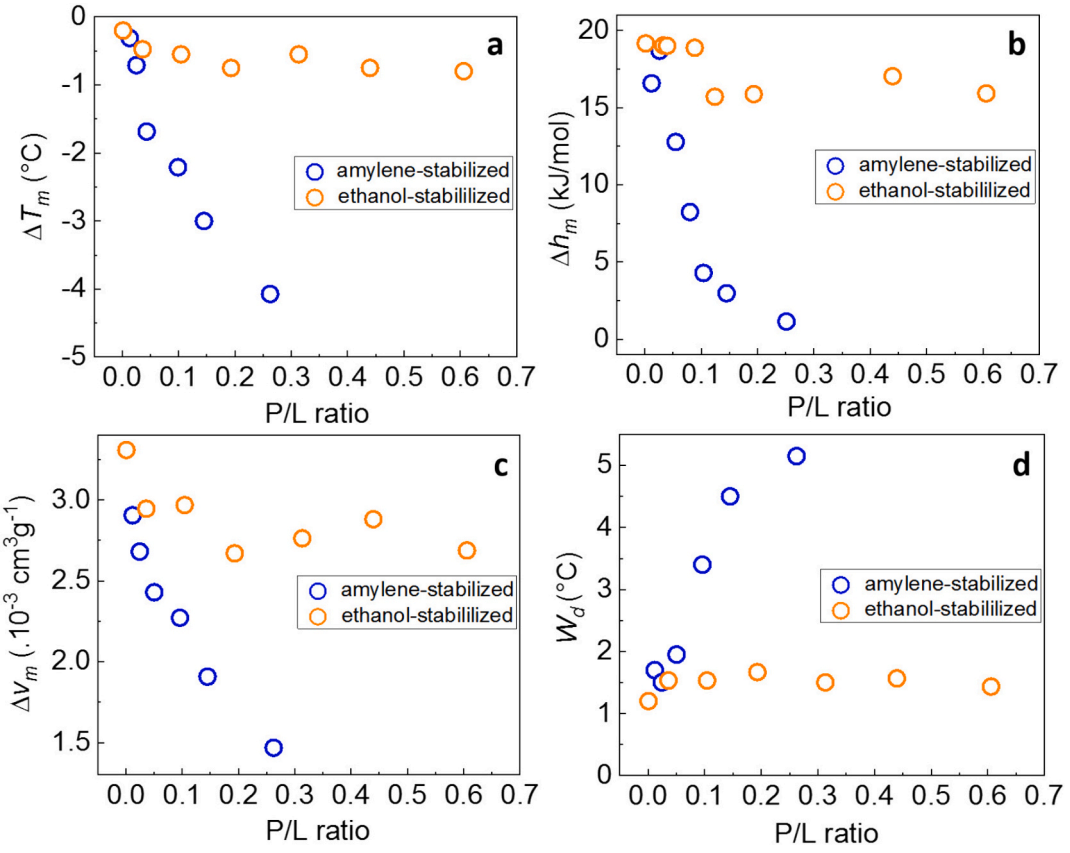

Fig. 2. Phase transition properties in bulk for the studied systems against the P/L ratio. Orange- chloroform stabilized with ethanol. Blue- chloroform stabilized with amylenes. **a)** Shift in transition temperature ΔT_m, **b)** transition enthalpy, Δh_m, **c)** transition volume Δv_m and **d)** width of the transition W_d. (For interpretation of the references to colour in this figure legend, the reader is referred to the web version of this article.)

difference in volume and enthalpy between the gel and liquid phases becomes smaller. This indicates that the gel phase becomes more similar to the liquid phase, *i.e.*, more liquid-like and, consequently, more disordered. Moreover, W_d, which provides information about the phase transition cooperativity (where a lower W_d indicates higher cooperativity), shows a significantly greater increase in samples containing amylene. Therefore, the interaction between amylene and Phe-Phe plays an important role, weakening the membrane to a much larger extent than when this alkene is absent. As a matter of fact, amylene or ethanol stabilizers do not change the phase transition of pure DMPC (in the absence of Phe-Phe). Melting temperatures, enthalpies, volumes and width of the phase transition are, within the experimental uncertainty, the same, irrespective of the chloroform stabilizer when there is no Phe-Phe in the sample.

For completeness, changes in the structural organization of the lipid molecules due to the incorporation of the Phe-Phe peptide were also evaluated for solid-supported vesicle layers. Phe-Phe/DMPC vesicle dispersions in MilliQ water were adsorbed onto Au-coated QCM-D sensors and their phase behavior assessed by calculating the temperature derivative of frequency shifts (see Fig. S2 in the SI). A general trend towards lower temperatures was obtained upon increasing P/L ratios, in good quantitative agreement with the above-exposed results for samples in bulk, obtained from calorimetry and densitometry.

At this point, it is worth noting that the amylene content in the chloroform is very small (200 ppm) and traces should be (in principle) removed from the samples upon film drying (boiling point ~37.5–38.5 °C). A plausible scenario where amylenes can associate with the pure peptide or form part of a three-component interaction with the Phe-Phe/DMPC mixture could explain the permanence of the alkene impurities in the studied systems. In the next sections, complementary nanomechanical, microscopy and ^{1}H NMR measurements are included to shed light into this hypothesis.

3.3. Topographic and nanomechanical characterization by AFM

AFM was used to gain insights into the impact of Phe-Phe over supported lipid bilayers (SLBs) formed from the rupture of vesicles prepared with amylene-stabilized chloroform. SLBs of Phe-Phe/DMPC mixtures were formed onto ultraflat SiO_2 single crystal surfaces at different P/L ratios (from 0.05 to 0.2), at 25 °C. At this temperature, we ensure that the measurements are conducted in the fluid phase (see Fig. 2 and **Fig. S2**). The corresponding membrane thicknesses are displayed in **Table S1** of the Supporting Information, where no statistically significant differences have been observed. Fig. 3 shows examples of AFM imaged areas for the SLBs under study. As it can be observed, the larger the P/L ratio, the more defects (bilayer pores) are present on the DMPC lipid bilayers. These are indicated in Fig. 3 by yellow arrows. These results differ from previously reported measurements of the same peptide /DMPC bilayers prepared using ethanol-stabilized chloroform, where almost no morphological changes were observed. [24]

Dynamic force spectroscopy measurements were also performed on Phe-Phe/DMPC SLBs at 0.05 and 0.1 P/L ratios in order to assess their nanomechanical properties. As depicted in Fig. 4, both systems display higher breakthrough forces with increasing approach speed v. Calculations on the k_0 values using Eq. 3 yield $k_{0,\ P/L=0.05} = 24 \pm 2$ Hz and $k_{0,\ P/L=0.1} = 69 \pm 3$ Hz. Changes in k_0 values are around the same magnitude as those obtained for SLBs exposed to pore-forming hydrophilic particles (*i.e.*, with k_0 increasing between 3- and 5- fold with respect to the pure lipid). [34]

From these results, it can be concluded that the probability of pore

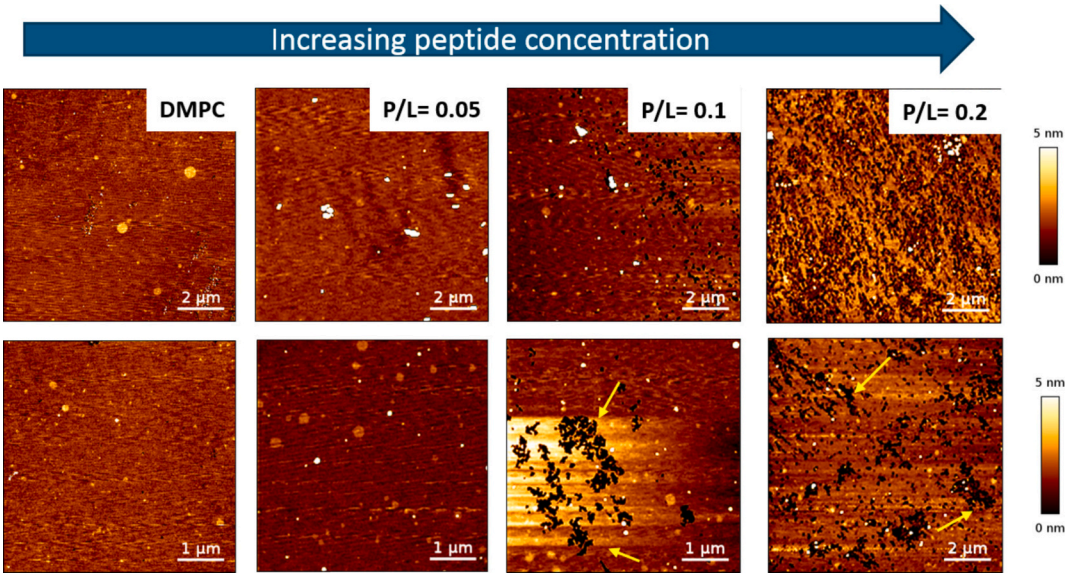

Fig. 3. AFM quantitative images of DMPC, and Phe-Phe/DMPC at P/L ratios of 0.05, 0.1, and 0.2. QI-AFM imaging was performed in water onto mapping areas of 10 (upper panels) and 5 μm^2 (lower panels) avoiding any surface dewetting that could cause spontaneous hole formation or lipid aggregation. All the data were obtained with films prepared in amylene-stabilized chloroform solutions. Bilayer pores are indicated by yellow arrows. (For interpretation of the references to colour in this figure legend, the reader is referred to the web version of this article.)

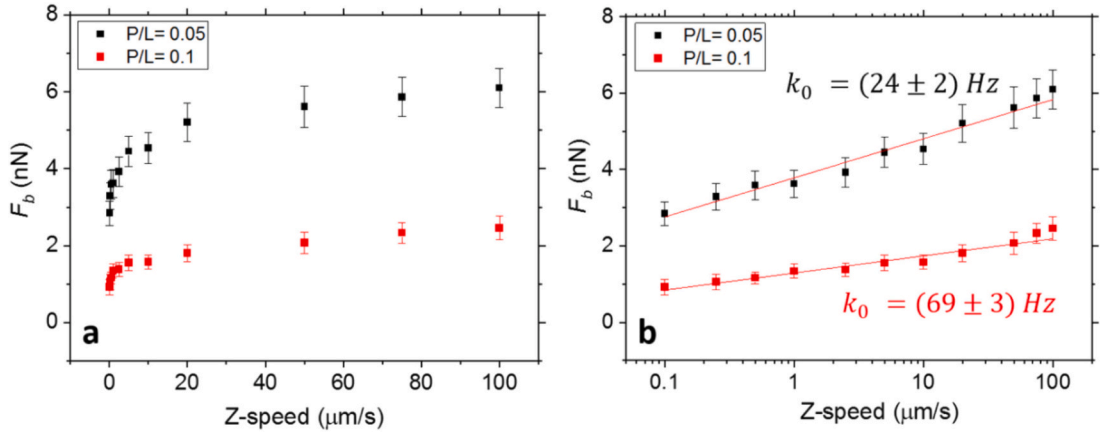

Fig. 4. AFM-DFS (Dynamic Force Spectroscopy) performed on supported Phe-Phe/DMPC mixed bilayers formed on SiO_2 wafers. **a)** Dependence of the tip approach speed on the breakthrough force values obtained for the 0.05 and 0.1 P/L ratios. **b)** F_b vs tip approach speed in semi logarithmic scale along with the estimated values for the probability of rupture (k_0) for each SLB film.

formation increases with increasing P/L ratio. This indicates that the bilayers loose nanomechanical stability and become less compact and more disordered, in agreement with the results obtained from interfacial and thermodynamic characterization of monolayers and multilamellar vesicles, respectively.

For microscopy and NMR characterization the peptide to lipid ratio P/L = 0.1 was kept constant, while varying the amount of chloroform used during the preparation of vesicles. As a result, the lipid and peptide concentrations are fixed, changing the amount of amylene present before the evaporation of the solvent in the lipid film. Table 2 provides an overview of all the samples studied by microscopy and NMR. We use a code for referring to the samples: Am and Et abbreviations specify the use of amylene or ethanol-stabilized chloroform. GV refer to samples prepared using the methodology described in section 2, with a large volume of chloroform. No GV suffix indicates that the sample was prepared using a small volume of chloroform (around twenty times smaller), implying lower amylene concentration. Samples prepared using a small chloroform volume were also characterized using thermodynamic and nanomechanical techniques. An intermediate behavior, between ethanol and high amylene content samples was observed. Thus, no relevant insights could be extracted from these data and we decided not to include them for the sake of clarity.

Table 2
Description of the samples measured using microscopy and NMR. P/L = 0.1 for the samples with Phe-Phe. Amylene concentration in the chloroform solution in mg per DMPC mg are also given.

	Description	Amylene concentration
DMPC-Am	Cl_3CH-amylene in small volume	0.035
PhDMPC-Et	Cl_3CH -EtOH	0
PhDMPC-Am	Cl_3CH-amylenes in small volume	0.035
PhDMPC-AmGV	Cl_3CH-amylenes in great volume	0.170
Ph-AmGV	Cl_3CH-amylenes in great volume	0.170
Ph-Am	Cl_3CH-amylenes in small volume	0.035

3.4. Microscopy of vesicles

Bright-Field Optical Microscopy (BFOM), Confocal Laser Scanning Microscopy (CLSM), and Transmission Electronic Microscopy (TEM) were used to get a multiscale picture of the shape and size of vesicles in bulk. BFOM was carried out without staining or vesicle immobilization. Panels **a-d** in Fig. 5 display the micrographs of DMPC vesicles without Phe-Phe (panel **a**) and three samples containing vesicles DMPC/PhePhe mixtures at P/L = 0.1 prepared under different conditions. No significant dissimilarities in the size distribution were observed among the samples, being all very polydisperse. Yet, while DMPC-Am and PhDMPC-Et samples consist of almost uniformly distributed isolated vesicles (panels **a** and **b**), PhDMPC-Am and PhDMPC-AmGV (panels **c** and **d**) display mostly clusters of aggregated vesicles, with regions where there are almost no vesicles. This shows that the combined presence of Phe-Phe and amylenes in the system induces vesicle aggregation. Increasing amylene concentration leads to lower packing of the aggregated vesicles [cfr **Figure (g,k)** *vs.* **(h,l)**].

Two fluorescent probes were used in confocal microscopy CLSM, namely rhodamine B, which interacts with the phospholipids membrane, [35] and Fast Green FCF, which associates to proteins [36], including the Phe-Phe peptide, as confirmed by preliminary experiments and by panels **e-l** of Fig. 5. Thus, they allow to disclose (globally) the distribution of the Phe-Phe dipeptide molecules in the DMPC bilayer structures. [37] Results are summarized in Fig. 5 (panels **e-l**) and reveal that Phe-Phe is located in the DMPC bilayer as FCF surrounds the vesicles (Fig. 5, **j-l**). CLSM and BFOM images show consistent results, namely isolated vesicles in DMPC-Am and PhDMPC-Et samples and clear aggregation in PhDMPC-Am and PhDMPC-AmGV ones.

An additional picture of the vesicle structure and distribution at a smaller scale was obtained by TEM microscopy, where the vesicles have undergone a drying process before being introduced into the microscope. [38] Unlike the other two microscopic techniques, TEM might induce morphological changes to some extent. TEM micrographs are included in Fig. 6 and display as well a high degree of polydispersity. The TEM scale resolves the multilamellar structure of the vesicles (red arrows) in DMPC-Am, in PhDMPC-Et (smaller number of lamellae), and in PhDMPC-Am, whereas unilamellar vesicles were observed for PhDMPC-AmGV. Small Phe-Phe fibers can be also seen in all the samples containing Phe-Phe (parallel arrangement, green arrow in Fig. 6b) except for PhDMPC-AmGV. These fibers could be the footprint of the saturation of peptide in the system. Thus, Phe-Phe would be in dynamic equilibrium between the membrane, the aqueous solution and the crystalline form in fibers. Vesicles with the highest amylene content (PhDMPC-AmGV) would interact with Phe-Phe (see next section) inducing amylene-(Phe-Phe) associations which would inhibit the fiber generation.

3.5. Nuclear magnetic resonance

Fig. 7 shows an overview of the NMR spectra of the samples under study. Measurements were made at 15 (gel phase) and 30 °C (fluid phase). Spectra **a** and **g** correspond to pure DMPC vesicle dispersions that lack almost completely ^{1}H signals. This absence of ^{1}H peaks can be ascribed to the fact that vesicles are large, mostly multilamellar, and have a close-packed/tight bilayer organization, thus the mobility of the atoms of phospholipid molecules is greatly suppressed within the timescale of the NMR experiments. Therefore, DMPC ^{1}H signals broaden

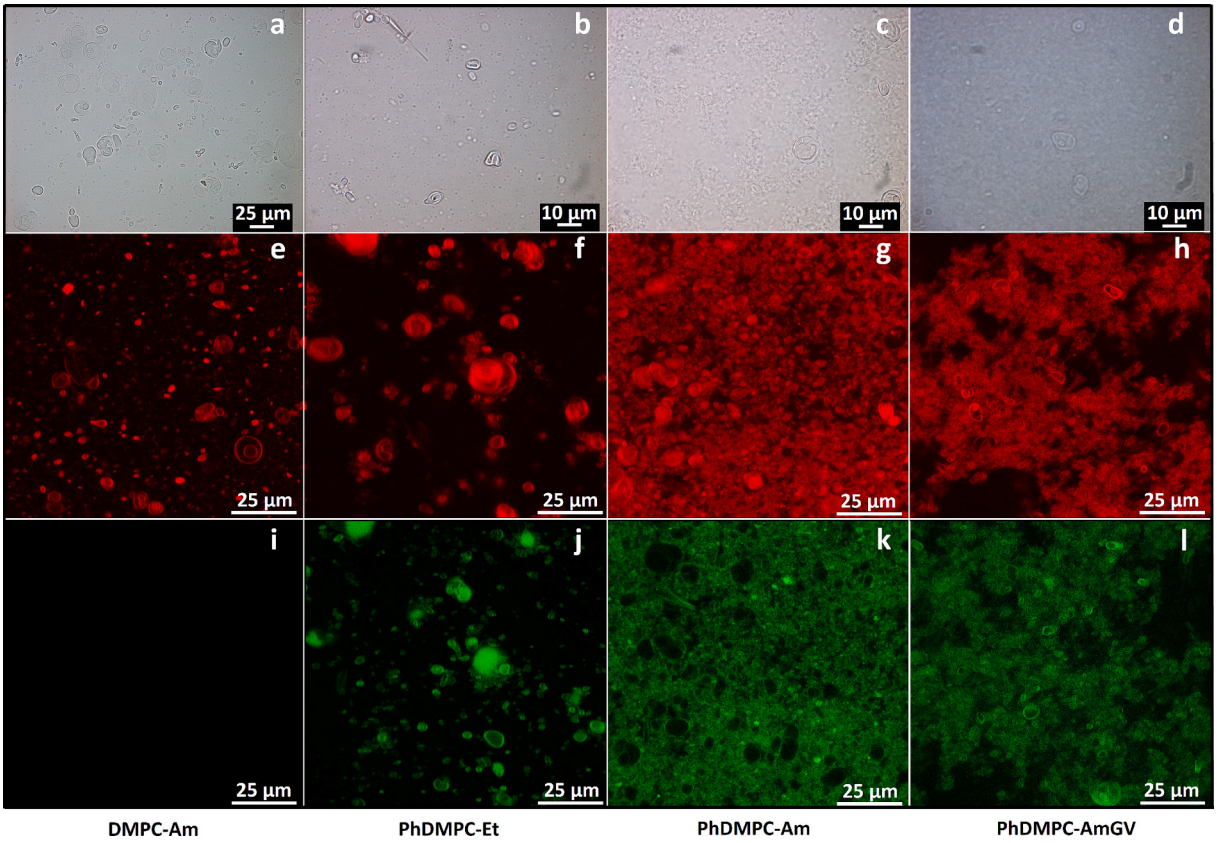

Fig. 5. Bright Field Optical Microscopy (BFOM, **a-d**) and Confocal Laser Scanning Microscopy (CLSM, **e-l**) images of DMPC-Am (**a, e, i**), PhDMPC-Et (**b, f, j**), PhDMPC-Am (**c, g, k**) and PhDMPC-AmGV (**d, h, l**). BFOM was performed without dyes inclusion and for all CLSM images the samples contain both Fast Green FCF (green colour) and Rhodamine B (red colour). Panels **e**–**h** were excited and collected at the Rhodamine B wavelengths (Materials and methods), and panels **i**–**l** at the Fast Green FCF wavelengths. No particle immobilization process was applied, and experiments were carried out at $T = 20$ °C. (For interpretation of the references to colour in this figure legend, the reader is referred to the web version of this article.)

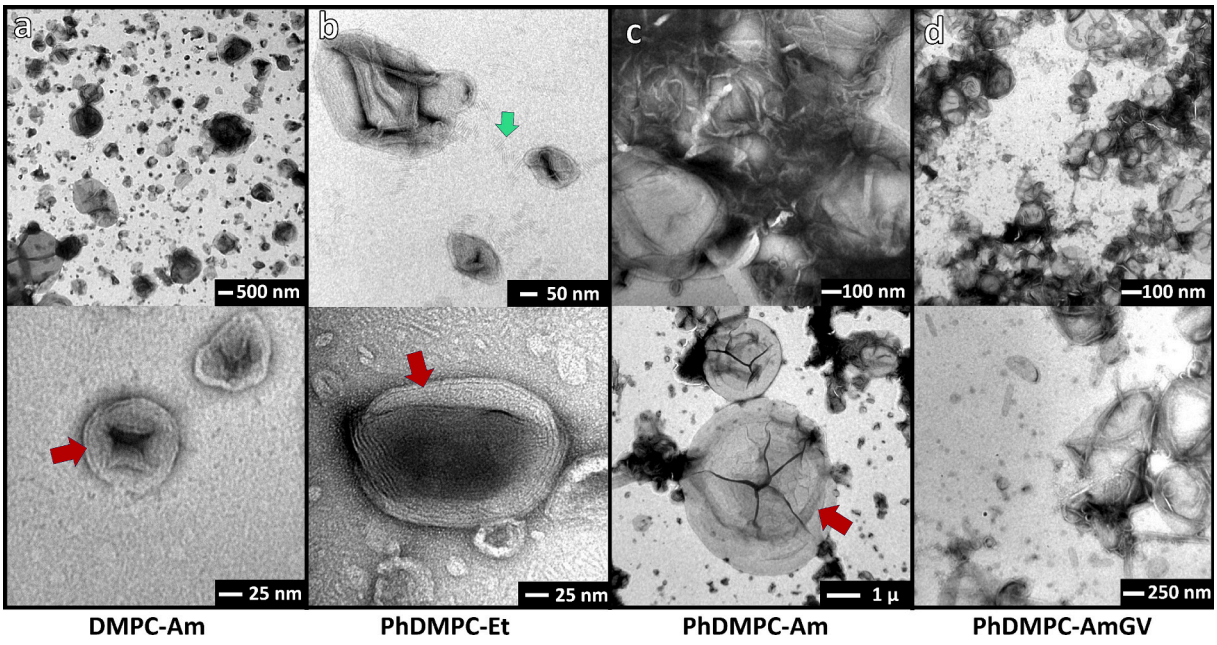

Fig. 6. TEM images of vesicles: a) DMPC-Am, b) PhDMPC-Et, c) PhDMPC-Am and d) PhDMPC-AmGV. a-c display multilamellar vesicles (red arrows). Green arrow points out Phe-Phe fibers. Experiments were carried out at $T = 20$ °C. (For interpretation of the references to colour in this figure legend, the reader is referred to the web version of this article.)

and drastically decrease in intensity when compared to the ^{1}H signals of isolated DMPC molecules in solution (see **Fig. S3**). [39,40] The only exception is the TMA peak at 3 ppm, visible at 30 °C (arrow 2 in spectrum **a**), revealing that some motion is allowed due to the fluidity of the lipid membrane in these conditions. It is relevant to highlight the differences between these spectra and those in the literature with clearer signals, although broad and poorly defined, for all the DMPC hydrogens. [41,42] This is mostly due to the fact that vesicle dispersions previously reported were homogenized to uniform sizes (less than 200 nm) and/or were unilamellar. [42,43]

The signal corresponding to amylene and indicated by the blue shadowed area of **panels c-f** and **h-l**, [44,45] is present only for the samples containing Phe-Phe. This is quite revealing and indicates that amylene must bind to the peptide, forming supramolecular complexes and preventing it to be removed from the lipid cake during the solvent evaporation. In the case of pure DMPC (panels **a** and **g**), two scenarios may be considered: i) either amylene fails to associate with DMPC and is thus lost during solvent evaporation resulting in no detectable signals or ii) amylene does interact with the hydrophobic (internal) regions of the membrane. In this latter case, the total absence of signals could be attributed to the same phenomenon that renders the signals from DMPC vesicles undetectable. However, this scenario is highly improbable, since the other techniques do not show any effect of amylene-DMPC interaction.

The different degree of widening and distortion of the Phe-Phe NMR signals across different samples can be easily visualized in Fig. 7. For vesicles prepared using ethanol-stabilized chloroform (Figs. 7b and h**)** spectra display a similar shape of that of pure Phe-Phe dissolved in water (**Fig. S4**). However, there is a strong distortion and widening of the Phe-Phe spectra for samples containing vesicles prepared using amylene-stabilized chloroform (**spectra c, d, i, j**). This is especially clear for the aromatic rings and β hydrogens (chemical shifts ~7.15 ppm and ~ 3 ppm at 15 °C, respectively), indicating that most of Phe-Phe molecules are in molecular configurations that strongly affect their mobility.

Chemical shifts in Fig. 7 can also provide relevant information. All functional groups show important variations with temperature with the exception of NH. This suggests that NH is somewhat protected from the increase of the environmental polarity with temperature, probably due to the Phe-Phe − DMPC interaction via the diphenylalanine carboxylate (negative charge) and the TMA of DMPC (positive charge). Moreover, the NH group is the only one that shows important chemical shift differences between samples. We will focus the discussion on the spectra recorded at 15 °C, since, with the already mentioned exception of the NH group, the spectra at 30 °C are basically the same as those of 15 °C, but slightly displaced towards larger chemical shifts. The NH signal chemical shift is 7.90 ppm for Phe-Phe dissolved in water (see **Fig. S4**), whereas it goes up to 8.03 ppm for the vesicles prepared using ethanol-stabilized chloroform (PhDMPC-Et, spectrum **h**). This value is quite similar to that observed for samples prepared with the lowest amylene concentration (8.05 ppm, see PhDMPC-Am, spectrum **j**). For pure Phe-Phe with the lowest amylene concentration (Ph-Am, spectrum **l**), the NH chemical shift goes up to 8.14 ppm. Therefore, low amylene concentration has a small effect over NH when diphenylalanine is mixed with DMPC, but quite strong when there is no DMPC in the sample. If the amylene concentration is raised, the NH shift goes up to 8.30 ppm for pure Phe-Phe (Ph-AmGV, spectrum **k**) and up to 8.32 ppm when mixed with DMPC (PhDMPC-AmGV, spectrum **i**). Thus, at high amylene concentrations, the above-observed tendency is reversed, and amylene affects slightly more the NH when there is DMPC in the sample.

These results together with those obtained using thermodynamic and nanomechanical characterization can help to envisage a molecular model for the studied systems, as depicted in Fig. 8. The NMR data reveals that diphenylalanine could form supramolecular complexes with amylene, which seemingly strongly affect the NH group. The possible options are a Phe-Phe-amylene dimer (Fig. 8a), a Phe-Phe-amylene-Phe-Phe trimer (Fig. 8b), the aromatic-amylene interaction being the most likely origin of both supramolecular arrangements, and a Phe-Phe-amylene-amylene-Phe-Phe cyclic tetramer (Fig. 8c). This latter configuration would facilitate the NH-carboxylate interaction in Phe-Phe, and would be responsible for the strong NH chemical shifts observed at high amylene concentrations (arrow 1). It must be pointed out that more complex configurations would be possible, but they would be nothing but a combination of those above exposed.

The diphenylalanine supramolecular complexes would be within a dynamic chemical equilibrium that is affected by the lipid membrane. At zero amylene concentration (thus in the absence of supramolecular

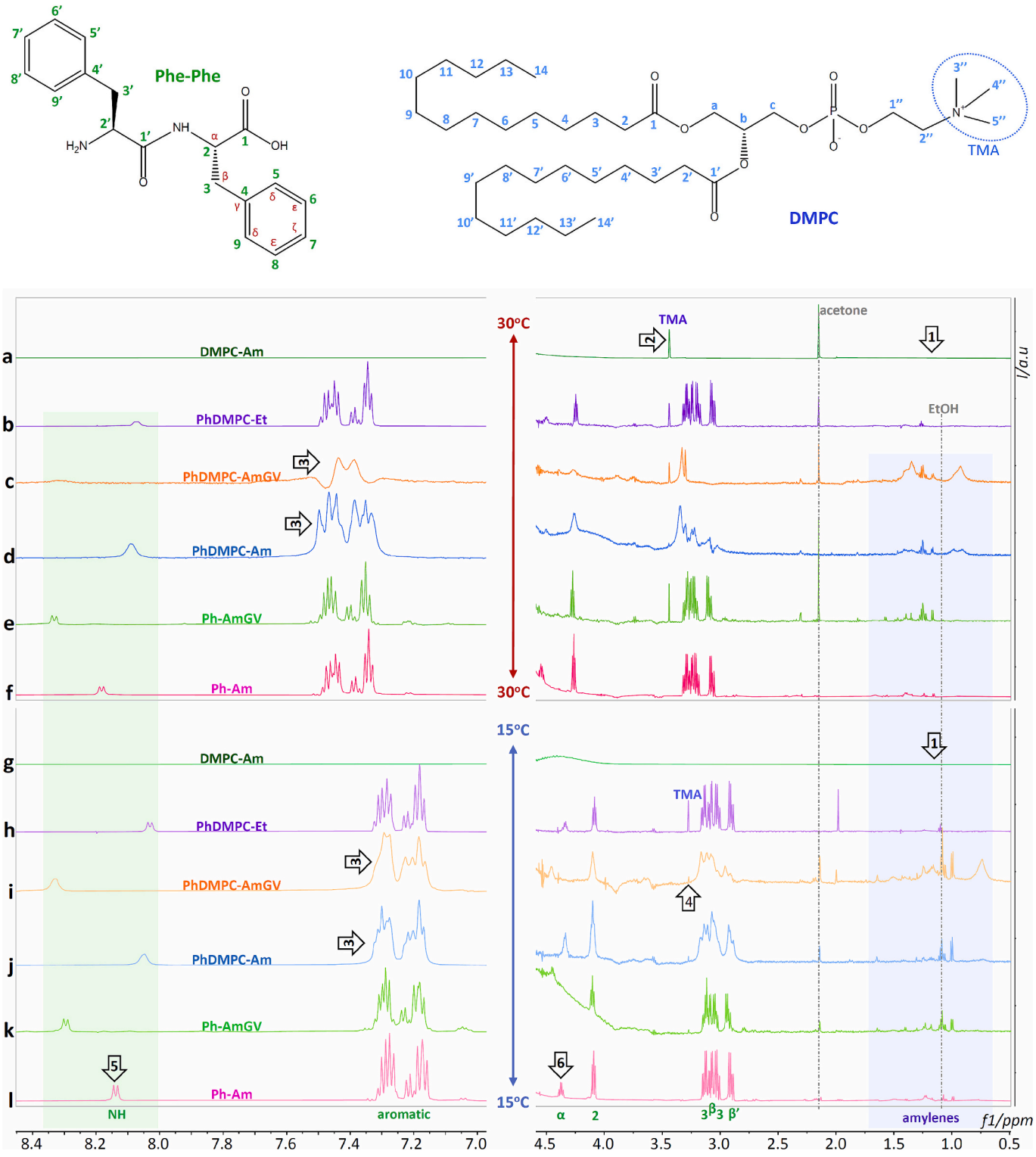

Fig. 7. ^{1}H NMR spectra of **a,g)** DMPC-Am, **b,h)** PhDMPC-Et, **c, i)** PhDMPC-AmGV, **d, j)** PhDMPC-Am, **e, k)** Ph-AmGV and **f, l)** Ph-Am. Light colours correspond to $T = 15$ °C and dark colours to $T = 30$ °C. Green labels correspond to Phe-Phe hydrogens, blue to DMPC, violet to amylene and grey labels indicate solvents. The samples were measured using a H_2O 95 % D_2O 5 % mixture as solvent. The green area represents the NH chemical shift range, and the blue area the main amylenes' range. (For interpretation of the references to colour in this figure legend, the reader is referred to the web version of this article.)

complexes), Phe-Phe would be attached to the membrane surface via a TMA-carboxylate bond (see Fig. 8e). At low amylene concentrations, the complexes would start to show up and act as bridges between lipid bilayers, resulting in the observed vesicle aggregation (see Fig. 8f). In both cases (zero or low amylene concentration), the NH group would interact with the phosphate group of DMPC, which would cause the similar NH chemical shifts observed for PhDMPC-Et and PhDMPC-Am (8.03 and 8.05 ppm, respectively). The higher value of the NH shift (8.14 ppm) for PhDMPC-Am could be caused by the equilibrium displacement towards the tetramer or more complex supramolecular structures when there is

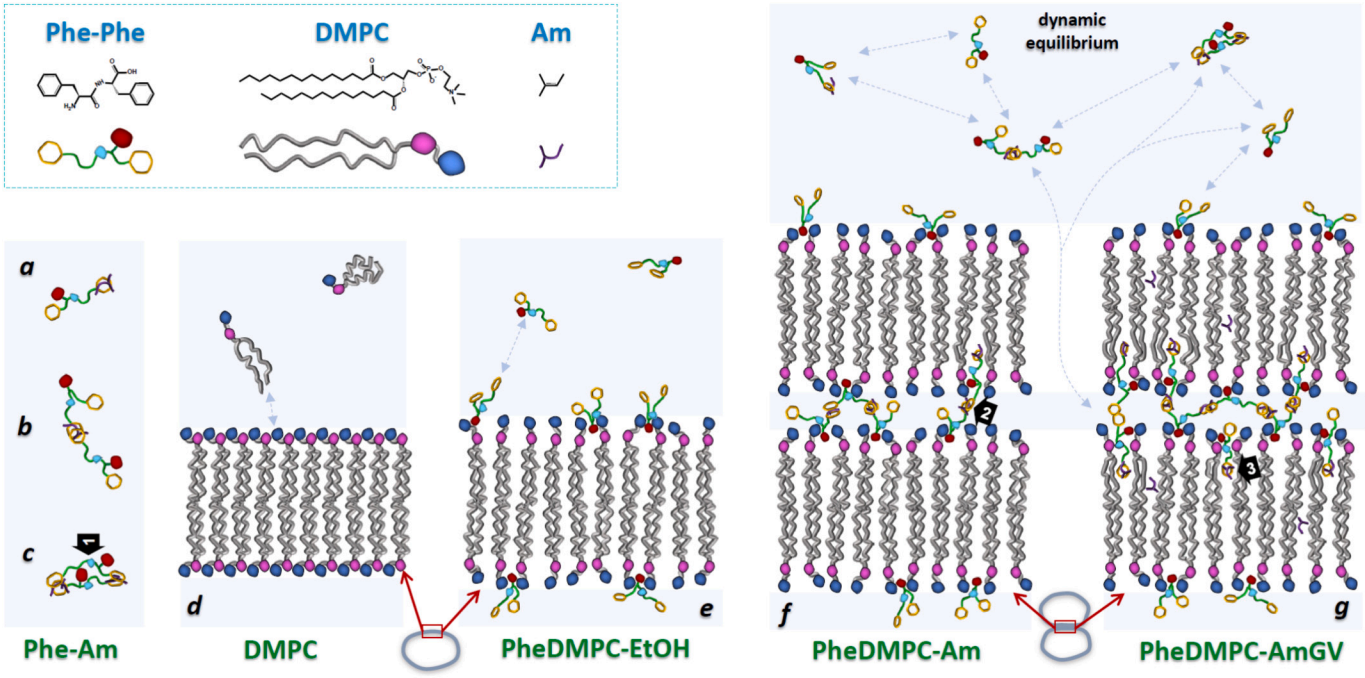

Fig. 8. Molecular picture proposed for vesicle-peptide interaction that explains the experimental results. **a-c)** Amylene-Phe-Phe supramolecular complexes. **d)** Pure DMPC bilayer. **e)** DMPC bilayer formed in ethanol-stabilized chloroform with diphenylalanine. **f)** DMPC bilayer formed in amylene-stabilized chloroform with diphenylalanine at low amylene concentration. **g)** DMPC bilayer formed in amylene-stabilized chloroform with diphenylalanine at high amylene concentration. Red and turquoise blobs represent the carboxylate and NH group of diphenylalanine whereas pink and blue ones are the phosphate and trimethylamine groups of DMPC. (For interpretation of the references to colour in this figure legend, the reader is referred to the web version of this article.)

no DMPC. Therefore, DMPC would act as a competitive inhibitor of these complexes through the TMA, which would bind the diphenylalanine carboxylate, and hampers the NH- carboxylate interactions between diphenylalanine molecules. On the other hand, the broadening and distortion of the NMR signals for PhDMPC-Am, as compared with PhDMPC-Et indicate that diphenylalanine-amylene complexes are more prone to interact with the lipid membrane. These complexes would be capable of integrating into the lipid fraction and forming bridges between adjacent vesicles, leading to vesicle aggregation (see Fig. 8f, arrow 2).

If the amylene concentration increases further, the equilibrium between the diphenylalanine complexes moves towards the formation of larger supramolecular structures (trimers, tetramers…). This would increase the ratio of diphenylalanine in the lipid membrane, increasing vesicle aggregation and weakening the membrane structure, reflected as a high distortion of the NMR signals (see Fig. 8g, arrow 3). In this respect, it is worth to point out that the high values obtained for the NH shift for PhDMPC-AmGV and Ph-AmGV (8.32 and 8.30 ppm, respectively) indicate that NH is located in a high polar environment. NH is thus probably linked to the phosphate group of DMPC or to the carboxylate of other diphenylalanine that forms the supramolecular complex. Additionally, these similar NH chemical shifts for PhDMPC-AmGV and Ph-AmGV suggest that the lipid membrane does not influence the equilibrium between the different diphenylalanine complexes dispersed in the aqueous solvent at such high amylene concentrations, in contrast to the results observed at low amylene concentrations.

4. Conclusions

The impact of diphenylalanine on the integrity and aggregation of zwitterionic DMPC lipid vesicles prepared in the presence and absence of amylene chloroform stabilizers was evaluated. The peptide concentration dependence was studied using thermodynamic and nanomechanical characterization. Experiments with lipid monolayers showed that both the expansion (increase of the area per molecule) and film fluidization effects caused by the peptide are enhanced in the presence of amylenes. Similarly, the main phase transition of DMPC is shifted towards lower temperatures and becomes less cooperative with increasing peptide concentration, the changes being much more pronounced in the presence of amylenes. Nanomechanical measurements by AFM dynamic force spectroscopy showed that bilayers display lower nanomechanical stability with increasing peptide concentration, being these membranes significantly weaker than the ethanol-stabilized chloroform counterparts.

Optical and TEM microscopies were employed to assess morphological changes in vesicles with a fixed P/L ratio of 0.1, a peptide concentration that shows significant changes in lateral organization, phase transition and nanomechanical stability as compared to pure DMPC bilayers. Microscopy images showed that samples without amylene consisted mostly of isolated vesicles, while vesicle aggregation was observed for vesicles prepared in the presence of both diphenylalanine and amylene. It is worth mentioning that aggregation was not observed for pure DMPC vesicles prepared in the presence of amylene stabilizer, indicating that amylenes alone do not induce vesicle aggregation if the peptide is not present.

A plausible molecular model on vesicle aggregation was proposed by ^{1}H NMR measurements. In the absence of amylene, Phe-Phe peptide molecules interact with the outermost part of the membrane, locating at the headgroup aqueous interface and leading to mild bilayer disorder. Conversely, the synergic action of amylene and Phe-Phe manifests in a concentration-dependent manner. While low amounts of amylene induce vesicle aggregation by bridging bilayers of apposing membranes −likely mediated by amylene and Phe-Phe supramolecular structures−, high amylene concentrations allow the diphenylamine-amylene complexes to disrupt the bilayer organization, leading to a greater degree of disorder. Vesicles consisting of more disordered bilayers are more prone to deform and will likely promote stronger aggregation (along a larger contact area), as observed by optical and TEM microscopy.

In summary, aggregation between zwitterionic vesicles can be straightforwardly achieved by a synergistic interaction of small alkenes

and peptides. These results will certainly motivate complementary computer simulations to unravel the molecular mechanisms behind combined action of both the dipeptide and the alkene, and serve as a reference for exploring other small molecules prone to display a similar combined effect. It will pave the way towards programmable aggregation by controlling the type and amount of aggregation agents.

CRediT authorship contribution statement

Martín Eduardo Villanueva: Writing – review & editing, Visualization, Supervision, Software, Resources, Methodology, Investigation, Formal analysis, Data curation. **Jacobo Troncoso:** Writing – review & editing, Writing – original draft, Visualization, Supervision, Project administration, Methodology, Investigation, Funding acquisition, Data curation, Conceptualization. **Patricia Losada-Pérez:** Writing – review & editing, Validation, Software, Resources, Methodology, Investigation, Funding acquisition, Formal analysis, Data curation, Conceptualization. **Aida Jover:** Writing – original draft, Visualization, Supervision, Resources, Methodology, Investigation, Funding acquisition, Formal analysis, Data curation.

Declaration of competing interest

The authors declare that they have no known competing financial interests or personal relationships that could have appeared to influence the work reported in this paper.

Acknowledgements

Support from the Spanish Ministry of Science, Innovation, and Universities under Grants No. PID2020-115722GB-C22 and PID2023-147148NB-I00 are greatly acknowledged. Support from the project 'DELTA' with project number 40008129 by 'Fonds de la Recherche Scientifique' (FNRS). M.E.V is a Collaborateur Scientifique of the Fonds de la recherche scientifique- FNRS. A. J. acknowledges A. López Greco for his help in the model discussion.

Appendix A. Supplementary data

Supplementary data to this article can be found online at https://doi.org/10.1016/j.molliq.2025.128596.

Data availability

Data will be made available on request.

References

[1] Y. Lu, G. Allegri, J. Huskens, Vesicle-based artificial cells: materials, construction methods and applications, Mater. Horiz. 9 (2022) 892–907, https://doi.org/10.1039/d1mh01431e.
[2] L. van der Koog, T.B. Gandek, A. Nagelkerke, Liposomes and extracellular vesicles as drug delivery systems: a comparison of composition, pharmacokinetics, and functionalization, Adv. Healthc. Mater. 11 (2022), https://doi.org/10.1002/adhm.202100639.
[3] V. Noireaux, A. Libchaber, A vesicle bioreactor as a step toward an artificial cell assembly, Proc. Natl. Acad. Sci. USA 101 (2004) 17669–17674, https://doi.org/10.1073/pnas.0408236101.
[4] J. Rizo, C. Rosenmund, Synaptic vesicle fusion, Nat. Struct. Mol. Biol. 15 (2008) 665–674, https://doi.org/10.1038/nsmb.1450.
[5] S.C. Harrison, Viral membrane fusion, Nat. Struct. Mol. Biol. 15 (2008) 690–698, https://doi.org/10.1038/nsmb.1456.
[6] K. Oorni, M.O. Pentikainen, M. Ala-Korpela, P.T. Kovanen, Aggregation, fusion, and vesicle formation of modified low density lipoprotein particles: molecular mechanisms and effects on matrix interactions, J. Lipid Res. 41 (2000) 1703–1714, https://doi.org/10.1016/s0022-2275(20)31964-7.
[7] K.J. Korshavn, C. Satriano, Y. Lin, R. Zhang, M. Dulchavsky, A. Bhunia, M. I. Ivanova, Y.H. Lee, C. La Rosa, M.H. Lim, A. Ramamoorthy, Reduced lipid bilayer thickness regulates the aggregation and cytotoxicity of amyloid-β, J. Biol. Chem. 292 (2017) 4638–4650, https://doi.org/10.1074/jbc.M116.764092.
[8] B.V. Derjaguin, L. Landau, Theory of the stability of strongly charged lyophobic sold and the adhesion of strongly charged particles in solutions of electrolytes, Acta Physicochim. URSS 14 (1941) 633–662.
[9] J.N. Israelachvili, Intermolecular and surface forces, third edit, academic press, Santa Barbara (2011), https://doi.org/10.1016/C2009-0-21560-1.
[10] S. Ohki, H. Ohshima, Interaction and aggregation of lipid vesicles (DLVO theory versus modified DLVO theory), Colloids Surf. B: Biointerfaces 14 (1999) 27–45, https://doi.org/10.1016/S0927-7765(99)00022-3.
[11] D. Saeki, S. Sugiura, T. Baba, T. Kanamori, S. Sato, S. Mukataka, S. Ichikawa, Dynamic interaction between oppositely charged vesicles: aggregation, lipid mixing, and disaggregation, J. Colloid Interface Sci. 320 (2008) 611–614, https://doi.org/10.1016/j.jcis.2007.12.002.
[12] H. Minami, I. Tohru, S. Ryosuke, Aggregation kinetics of Dimyristoylphosphatidylglycerol vesicles induced by divalent cations, J. Colloid Interface Sci. 158 (1993) 460–465, https://doi.org/10.1006/jcis.1993.1279.
[13] K. Suzuki, K. Kurihara, Y. Okura, T. Toyota, T. Sugawara, PH-induced switchable vesicular aggregation of zwitterionic and anionic phospholipids, Chem. Lett. 41 (2012) 1084–1086, https://doi.org/10.1246/cl.2012.1084.
[14] Y.-H.M. Chan, B. Van Lengerich, S.G. Boxer, Effects of Linker Sequences on Vesicle Fusion Mediated by Lipid-Anchored DNA Oligonucleotides. www.pnas.orgcgidoi10.1073pnas.0812356106, 2009.
[15] J.B. Massey, D.H. Bick, H.J. Pownall, Spontaneous transfer of monoacyl amphiphiles between lipid and protein surfaces, Biophys. J. 72 (1997) 1732–1743, https://doi.org/10.1016/S0006-3495(97)78819-2.
[16] J.E. Cummings, T.K. Vanderlick, Aggregation and hemi-fusion of anionic vesicles induced by the antimicrobial peptide cryptdin-4, Biochim. Biophys. Acta Biomembr. 1768 (2007) 1796–1804, https://doi.org/10.1016/j.bbamem.2007.04.016.
[17] K.L.H. Lam, H. Wang, T.A. Siaw, M.R. Chapman, A.J. Waring, J.T. Kindt, K.Y. C. Lee, Mechanism of structural transformations induced by antimicrobial peptides in lipid membranes, Biochim. Biophys. Acta Biomembr. 2012 (1818) 194–204, https://doi.org/10.1016/j.bbamem.2011.11.002.
[18] L. Milanesi, T. Sheynis, W.F. Xue, E.V. Orlova, A.L. Hellewell, R. Jelinek, E. W. Hewitt, S.E. Radford, H.R. Saibil, Direct three-dimensional visualization of membrane disruption by amyloid fibrils, Proc. Natl. Acad. Sci. USA 109 (2012) 20455–20460, https://doi.org/10.1073/pnas.1206325109.
[19] H. Komatsu, S. Okada, Ethanol-Induced Aggregation and Fusion of Small Phosphatidylcholine Liposome: Participation of Interdigitated Membrane Formation in their Processes, 1995.
[20] S. Kundu, S. Malik, M. Ghosh, S. Nandi, A. Pyne, A. Debnath, N. Sarkar, A comparative study on DMSO-induced modulation of the structural and dynamical properties of model bilayer membranes, Langmuir 37 (2021) 2065–2078, https://doi.org/10.1021/acs.langmuir.0c03037.
[21] G.M. Dyson, Phosgene, Chem. Rev. 4 (1927) 109–165.
[22] C.H. Görbitz, The structure of nanotubes formed by diphenylalanine, the core recognition motif of Alzheimer's β-amyloid polypeptide, Chem. Commun. (2006) 2332–2334, https://doi.org/10.1039/b603080g.
[23] B.B. Gerbelli, E.R. Da Silva, B. Miranda Soares, W.A. Alves, E. Andreoli De Oliveira, Multilamellar-to-Unilamellar transition induced by diphenylalanine in lipid vesicles, Langmuir 34 (2018) 2171–2179, https://doi.org/10.1021/acs.langmuir.7b03869.
[24] L. Bar, P. Losada-Pérez, J. Troncoso, Effect of diphenylalanine on model phospholipid membrane organization, J. Mol. Liq. 384 (2023) 122196, https://doi.org/10.1016/j.molliq.2023.122196.
[25] M.E. Villanueva, A.E. Lanterna, R.V. Vico, Hydrophobic silver nanoparticles interacting with phospholipids and stratum corneum mimic membranes in Langmuir monolayers, J. Colloid Interface Sci. 543 (2019) 247–255, https://doi.org/10.1016/j.jcis.2019.02.069.
[26] D. Fitzgerald, C. Du, S. Asaph, Technical Assessment of the Anton Paar DMA5000 Density Meter, United Kindom, 2000.
[27] E.W. Lemmon, M.O. McLinden, D.G. Friend, Thermophysical properties of fluid systems, in: P.J. Linstrom, W.G. Mallard (Eds.), NIST Chemistry WebBook, NIST Standard Reference Database Number 69, National Institute of Standards and Technology, Gaithersburg MD, 20899, USA, 1998, https://doi.org/10.18434/T4D303.
[28] S.K. Pramanik, S. Seneca, A. Ethirajan, S. Neupane, F.U. Renner, P. Losada-Pérez, Ionic strength dependent vesicle adsorption and phase behavior of anionic phospholipids on a gold substrate, Biointerphases 11 (2016) 019006, https://doi.org/10.1116/1.4939596.
[29] S. Neupane, Y. De Smet, F.U. Renner, P. Losada-Pérez, Quartz crystal microbalance with dissipation monitoring: a versatile tool to monitor phase transitions in biomimetic membranes, Front Mater 5 (2018) 1–8, https://doi.org/10.3389/fmats.2018.00046.
[30] E.L. Florin, M. Rief, H. Lehmann, M. Ludwig, C. Dornmair, V.T. Moy, H.E. Gaub, Sensing specific molecular interactions with the atomic force microscope, Biosens. Bioelectron. 10 (1995) 895–901, https://doi.org/10.1016/0956-5663(95)99227-C.
[31] H.J. Butt, V. Franz, Rupture of molecular thin films observed in atomic force microscopy. I. Theory, Phys. Rev. E Stat. Phys. Plasmas Fluids Relat. Interdiscip. Topics 66 (2002) 1–9, https://doi.org/10.1103/PhysRevE.66.031601.
[32] J. Asadi, S. Ferguson, H. Raja, C. Hacker, P. Marius, R. Ward, C. Pliotas, J. Naismith, J. Lucocq, Enhanced imaging of lipid rich nanoparticles embedded in methylcellulose films for transmission electron microscopy using mixtures of heavy metals, Micron 99 (2017) 40–48, https://doi.org/10.1016/j.micron.2017.03.019.
[33] J.T. Davies, E.K. Rideal, Interfacial Phenomena, Second, Academic Press, London, 1963.

[34] M.E. Villanueva, L. Bar, L. Porcar, Y. Gerelli, P. Losada-Pérez, Resolving the interactions between hydrophilic CdTe quantum dots and positively charged membranes at the nanoscale, J. Colloid Interface Sci. 677 (2025) 620–631, https://doi.org/10.1016/j.jcis.2024.07.220.
[35] N. Magalhães, G.M. Simões, C. Ramos, J. Samelo, A.C. Oliveira, H.A.L. Filipe, J.P. P. Ramalho, M.J. Moreno, L.M.S. Loura, Interactions between rhodamine dyes and model membrane systems—insights from molecular dynamics simulations, Molecules 27 (2022) 1420, https://doi.org/10.3390/molecules27041420.
[36] C.M. Wilson, Studies and critique of amido black 10B, Coomassie blue R, and fast green FCF as stains for proteins after polyacrylamide gel electrophoresis, Anal. Biochem. 96 (1979) 263–278, https://doi.org/10.1016/0003-2697(79)90581-5.
[37] S. Gallier, D. Gragson, R. Jiménez-Flores, D. Everett, Using confocal laser scanning microscopy to probe the milk fat globule membrane and associated proteins, J. Agric. Food Chem. 58 (2010) 4250–4257, https://doi.org/10.1021/jf9032409.
[38] N. Koifman, Y. Talmon, Cryogenic electron microscopy methodologies as analytical tools for the study of self-assembled pharmaceutics, Pharmaceutics 13 (2021), https://doi.org/10.3390/pharmaceutics13071015.
[39] R.J. Gillams, J.V. Busto, S. Busch, F.M. Goñi, C.D. Lorenz, S.E. McLain, Solvation and hydration of the ceramide headgroup in a non-polar solution, J. Phys. Chem. B 119 (2015) 128–139, https://doi.org/10.1021/jp5107789.
[40] M. Delcea, S. Moreno-Flores, D. Pum, U.B. Sleytr, J.L. Toca-Herrera, On the lipid-bacterial protein interaction studied by quartz crystal microbalance with dissipation, transmission electron microscopy and atomic force microscopy. http://arxiv.org/abs/0904.1662, 2009.
[41] G. Da Costa, L. Mouret, S. Chevance, E. Le Rumeur, A. Bondon, NMR of molecules interacting with lipids in small unilamellar vesicles, Eur. Biophys. J. 36 (2007) 933–942, https://doi.org/10.1007/s00249-007-0186-7.
[42] C. Schwieger, A. Achilles, S. Scholz, J. Rüger, K. Bacia, K. Saalwaechter, J. Kressler, A. Blume, Binding of amphiphilic and triphilic block copolymers to lipid model membranes: the role of perfluorinated moieties, Soft Matter 10 (2014) 6147–6160, https://doi.org/10.1039/c4sm00830h.
[43] S.V. Dvinskikh, V. Castro, D. Sandström, Efficient solid-state NMR methods for measuring heteronuclear dipolar couplings in unoriented lipid membrane systems, Phys. Chem. Chem. Phys. 7 (2005) 607–613, https://doi.org/10.1039/b418131j.
[44] Z. Zhang, T. Xiao, H. Al-Megren, S.A. Aldrees, M. Al-Kinany, V.L. Kuznetsov, M. L. Kuznetsov, P.P. Edwards, Hydrogen bonds between methanol and the light liquid olefins 1-pentene and 1-hexene: from application to fundamental science, Chem. Commun. 53 (2017) 4026–4029, https://doi.org/10.1039/c6cc09545c.
[45] V. Bellière, C. Lorentz, C. Geantet, Y. Yoshimura, D. Laurenti, M. Vrinat, Kinetics and mechanism of liquid-phase alkylation of 3-methylthiophene with 2-methyl-2-butene over a solid phosphoric acid, Appl Catal B 64 (2006) 254–261, https://doi.org/10.1016/j.apcatb.2005.11.011.